

UV-Induced Isomerization Dynamics of *N*-Methyl-2-Pyridone in Solution

Daniel Murdock,¹ Stephanie J. Harris,¹ Ian P. Clark,² Gregory M. Greetham,² Michael Towrie,² Andrew J. Orr-Ewing,¹ and Michael N. R. Ashfold¹

¹School of Chemistry, University of Bristol, Cantock's Close, Bristol, BS8 1TS, United Kingdom.

²Central Laser Facility, Research Complex at Harwell, Science and Technology Facilities Council, Rutherford Appleton Laboratory, Didcot, Oxfordshire, OX11 0QX, United Kingdom

Supporting Information

A. Static FTIR and UV/vis spectra

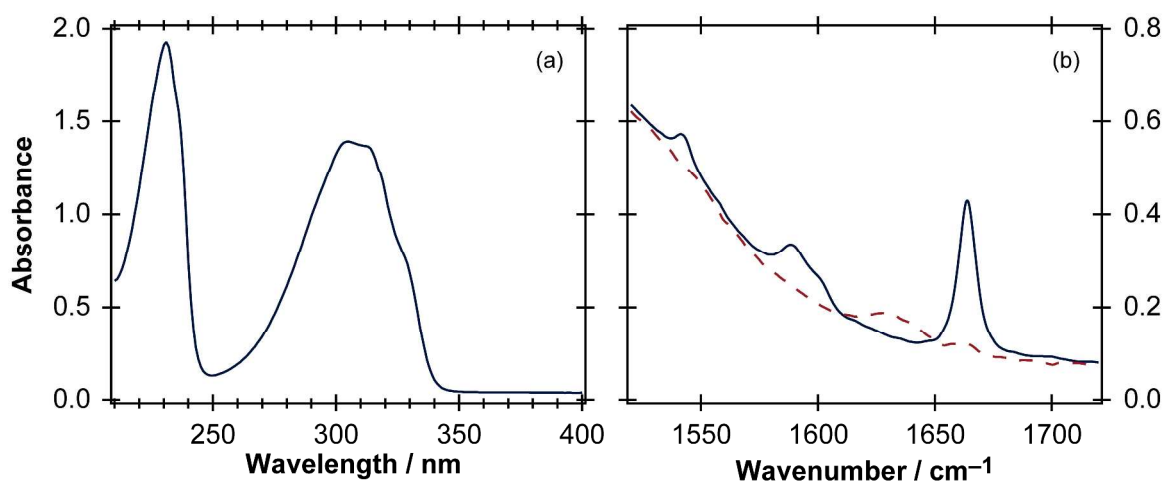


Figure S1. (a) UV/visible and (b) FTIR spectrum of a 30 mM solution of NMP/CH₃CN, recorded using a 100 μ m pathlength Harrick Cell. The dashed line in panel (b) is the solvent signal.

B. Decomposition of spectra in terms of model functions

(i) Carbonyl stretch region ($\lambda_{pump}=267\text{ nm}$)

The four parent bleaches were modeled as a sum of Lorentzian-type features (Bleach in fig S2):

$$y(x) = P \sum_n \frac{A_n}{(x - x_n)^2 + B_n}$$

with the global best-fit peak centers (x_n), widths (B_n), and relative amplitudes (A_n) obtained from a simultaneous fit to all the available data. The overall amplitude (P) was allowed to float for the fit to each individual time-slice, with this parameter providing a measure of the parent molecule population. The overlapping gain signals arising from S_1 molecules were modeled as Gaussian-type features:

$$y(x) = A \exp \left\{ - \left(\frac{x - x_0}{w} \right)^2 \right\}$$

where the $<1540\text{ cm}^{-1}$ (G1) and $1560\text{--}1580\text{ cm}^{-1}$ (G2) peaks had globally fit peak centers and widths (amplitude allowed to float freely), while all fit parameters were allowed to float for the $1620\text{--}1660\text{ cm}^{-1}$ feature (G3).

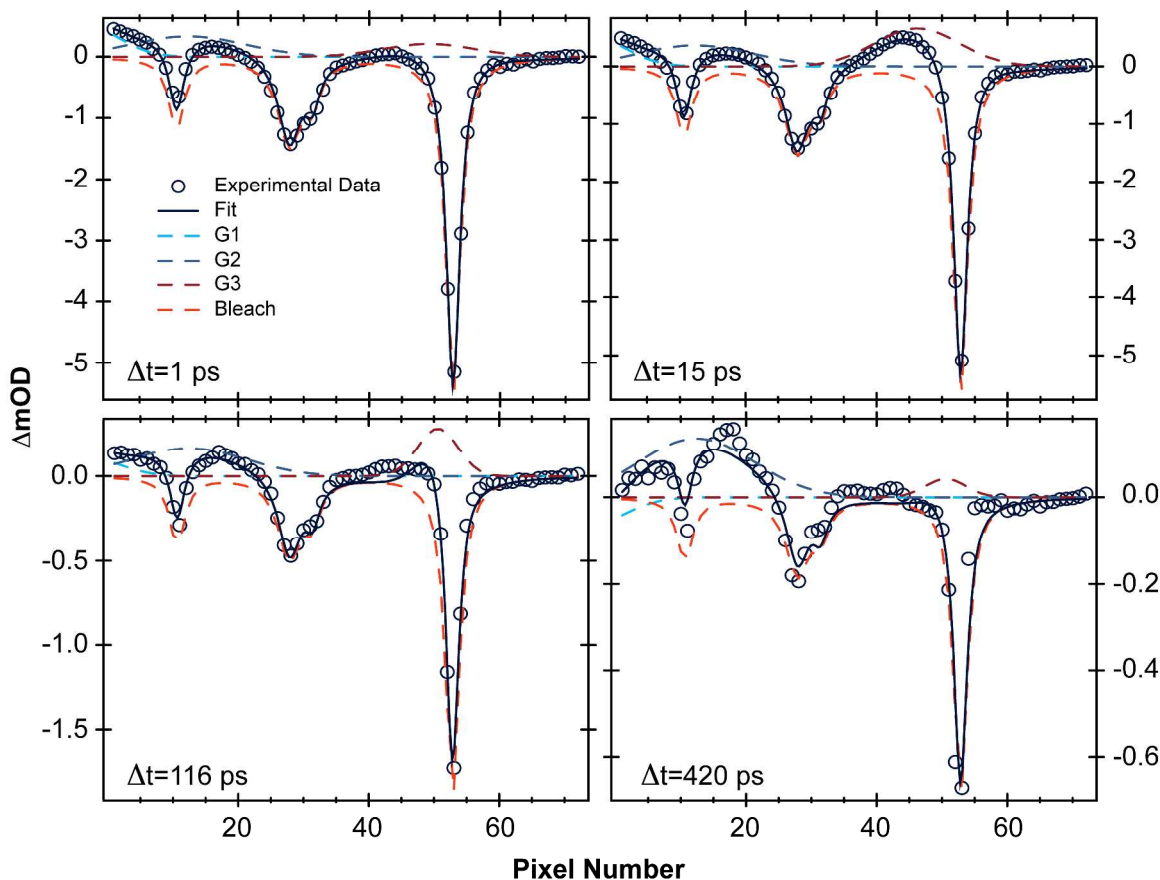


Figure S2. Decomposition of a series of 267 nm pump, carbonyl probe, TVA spectra in terms of model functions.

(ii) Ketene stretch region ($\lambda_{pump}=267$ nm)

The vibrationally cold ketene features were modeled using Lorentzian functions (L1 and L2, respectively, in figure S3), while the vibrationally hot signal seen at early times is described as a Gaussian (G1). The peak centers and widths of all model functions were constrained to their global best-fit values, while the amplitudes were allowed to float freely. The time-dependent areas, rather than the amplitudes, of each of the basis functions are used in the kinetic fits.

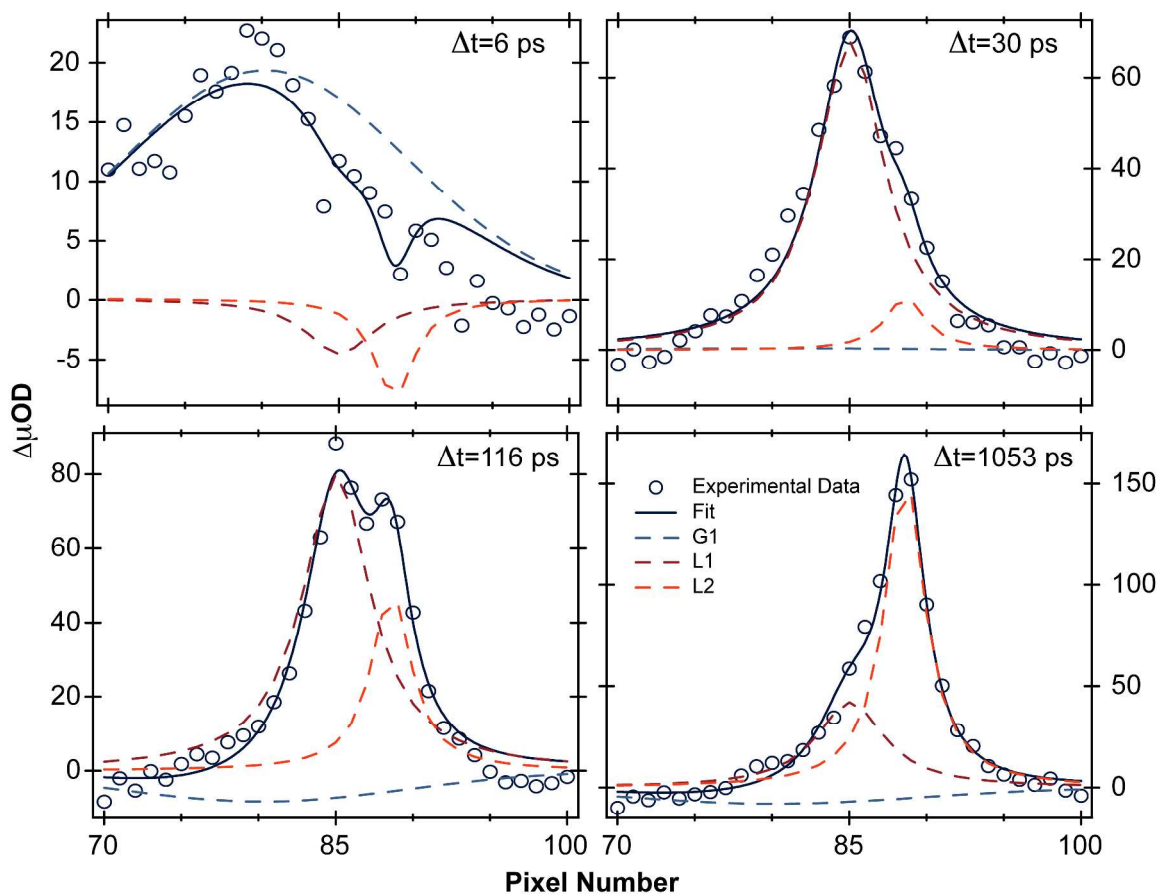


Figure S3. Decomposition of a series of 267 nm pump, ketene probe, TVA spectra in terms of model functions.

(iii) Ketene stretch region ($\lambda_{pump}=330$ nm)

The vibrationally cold ketene features were modeled using Lorentzian functions (L1 and L2, respectively, in figure S4). The peak centers and widths of both Lorentzians were constrained to their global best-fit values, while the amplitudes were allowed to float freely. The time-dependent areas, rather than the amplitudes, of each of the basis functions are used in the kinetic fits.

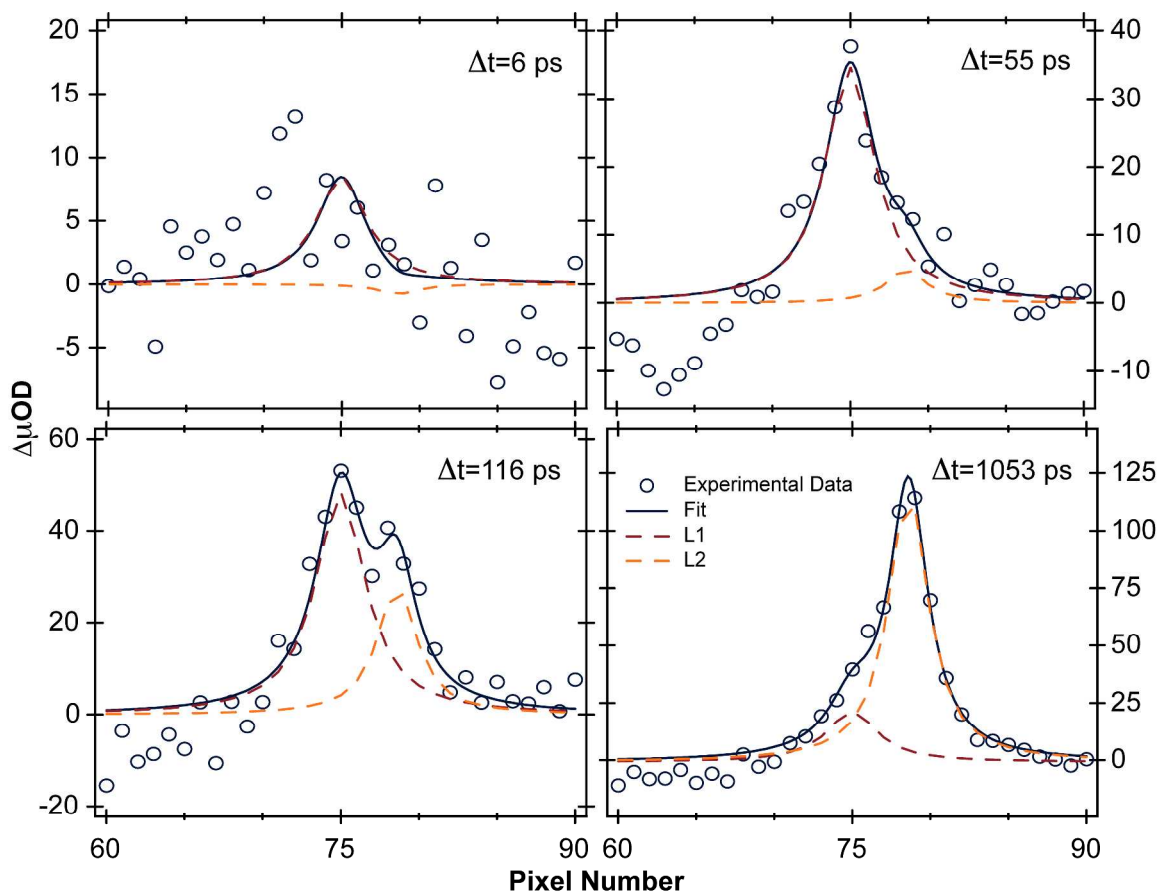


Figure S4. Decomposition of a series of 330 nm pump, ketene probe, TVA spectra in terms of model functions.

C. Early time bleach dynamics

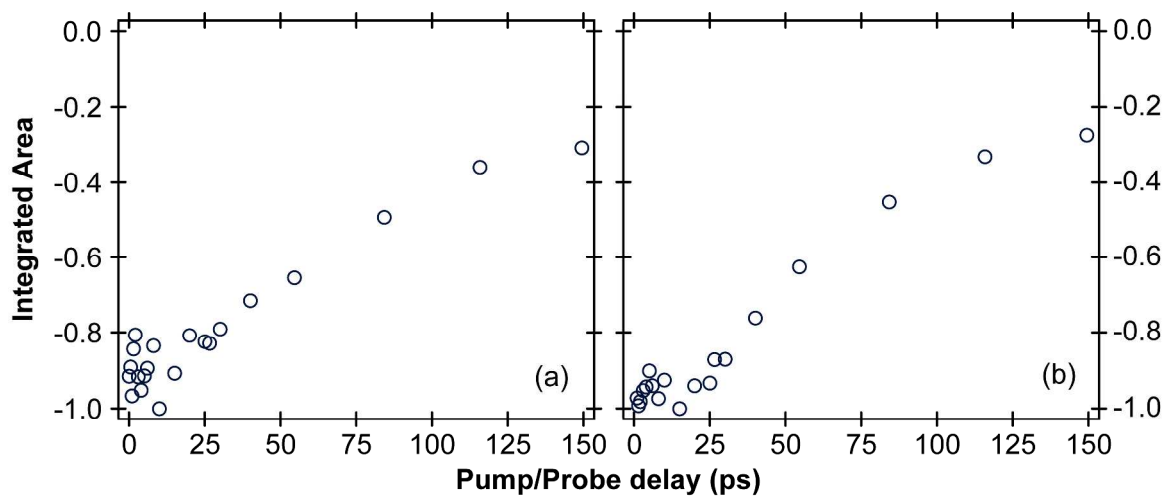


Figure S5. Early-time NMP(S_0) bleach kinetics following excitation at (a) 330 nm, and (b) 267 nm, highlighting the ~ 20 ps delay before the parent molecule population begins to recover.

D. Anharmonic wavenumber calculations

Table S1. Anharmonic vibrational wavenumbers calculated for NMP, ketene1, and ketene2 at the MP2/6-311+G(*d,p*) level of theory.

NMP		ketene1		ketene2	
<i>Anharmonic Wavenumber (cm⁻¹)</i>	<i>Intensity (km mol⁻¹)</i>	<i>Anharmonic Wavenumber (cm⁻¹)</i>	<i>Intensity (km mol⁻¹)</i>	<i>Anharmonic Wavenumber (cm⁻¹)</i>	<i>Intensity (km mol⁻¹)</i>
3129.7	1	3128.7	5	3160.6	7
3114.1	3	3110.7	5	3118.3	0
3102.5	3	3037.3	13	3028.8	14
3061.8	2	2998.6	21	2991.9	7
3080.2	6	2962.8	18	2937.0	34
3040.9	8	2876.5	41	2816.4	33
3005.8	22	2925.6	29	2799.0	63
1710.1	288	2142.8	323	2132.9	354
1618.3	31	1599.0	32	1569.5	7
1550.8	30	1482.6	10	1483.0	4
1491.5	7	1467.7	2	1480.1	5
1468.6	6	1461.6	1	1467.1	0
1450.7	3	1434.6	1	1434.6	1
1426.2	2	1395.4	15	1405.6	3
1400.1	5	1339.8	13	1342.5	7
1339.4	24	1260.4	22	1298.4	12
1241.4	21	1243.6	31	1229.1	29
1185.0	8	1221.6	23	1215.3	14
1156.2	15	1137.6	6	1177.6	1
1137.2	0	1134.0	5	1130.8	17
1134.3	16	1119.6	4	1129.3	14
1056.9	20	1087.8	37	1085.6	11
1017.0	2	971.0	3	1012.6	5
1082.6	2	965.8	5	981.1	7
876.2	3	957.3	14	931.8	7
998.9	1	874.1	11	892.6	0
896.2	2	820.2	4	814.8	6
745.1	9	703.5	7	677.1	5
778.2	82	685.7	27	673.5	37
844.0	1	636.4	12	622.9	3
591.6	1	507.5	7	529.2	1
561.6	2	499.2	12	503.1	4
453.1	7	403.5	6	344.7	11
1088.8	30	371.9	1	356.1	4
463.9	104	300.7	2	338.6	1
348.1	4	224.7	1	246.3	1
326.3	16	178.3	9	177.4	4
156.0	5	140.8	3	140.1	2
270.1	27	42.8	1	53.1	0
<i>Energy (relative to NMP; zero point corrected)</i>		17260 cm ⁻¹		17430 cm ⁻¹	

E. CASSCF active space

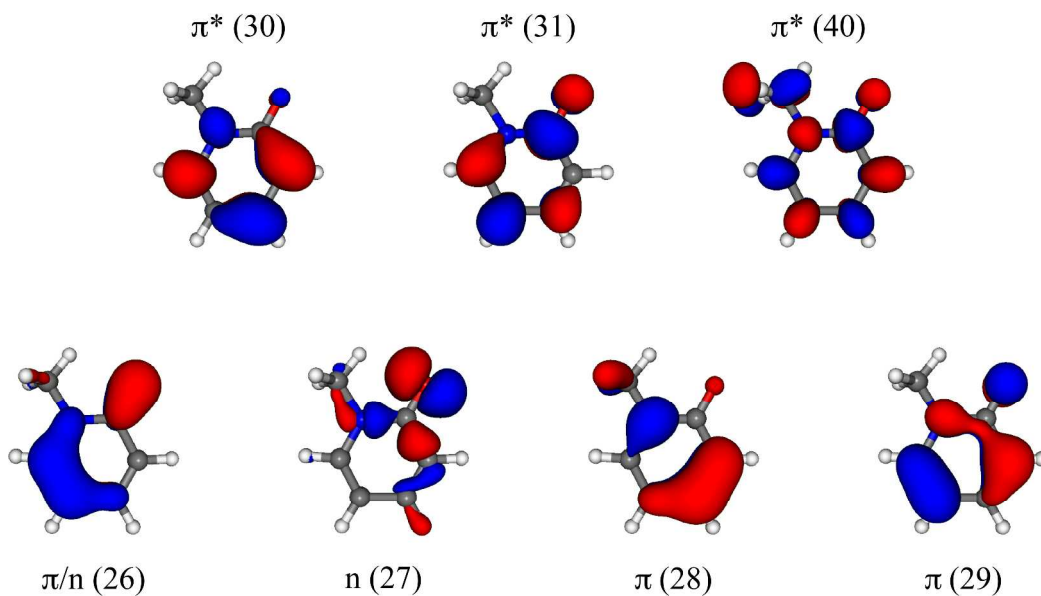


Figure S6. NMP molecular orbitals comprising the (8,7) active space used in the construction of the LIIC potential energy curves. The bonding orbitals are in the bottom half of the figure, with the non-bonding orbitals in the top half. Isolines are drawn at a value of 0.05.